Ground Truth Generation Algorithm for Medium-Frequency R-Mode Skywave Detection

Suhui Jeong
School of Integrated Technology
Yonsei University
Incheon, Korea
ssuhui@yonsei.ac.kr

Pyo-Woong Son*
Korea Research Institute of Ships and Ocean Engineering
Daejeon, Korea
Ship and Ocean Engineering Major
University of Science and Technology
Daejeon, Korea
pwson@kriso.re.kr
* Corresponding author

Abstract—With the advancement of transportation vehicles, the importance and utility of navigation systems providing positioning, navigation, and timing (PNT) information have been increasing. Global navigation satellite systems (GNSS) are widely used navigation systems, but they are vulnerable to radio frequency interference (RFI), resulting in disruptions of satellite navigation signals. Recognizing this limitation, extensive research is being conducted on alternative navigation systems. In the maritime industry, ongoing research focuses on a ground-based integrated navigation system called R-Mode. R-Mode utilizes medium frequency (MF) differential GNSS (DGNSS) and very high-frequency data exchange system (VDES) signals as ranging signals for positioning and incorporates the existing ground-based navigation system known as enhanced long-range navigation (eLoran). However, MF R-Mode, which uses MF DGNSS signals for positioning, exhibits significant performance differences between daytime and nighttime due to skywave interference caused by signals reflecting off the ionosphere. In this study, we propose a skywave ground truth generation algorithm that is crucial for studying mitigation methods for MF R-Mode skywave interference. Furthermore, we demonstrate the proposed algorithm using field-test data.

Index Terms—Medium-frequency (MF) R-Mode, skywave detection, ground truth generation

I. INTRODUCTION

In the era of the Fourth Industrial Revolution, the significance and applicability of navigation systems providing positioning, navigation, and timing (PNT) information are steadily increasing with the advancements in sophisticated modes of transportation, such as autonomous ships, autonomous vehicles, and urban air mobility (UAM). This importance is particularly evident in the marine environment, where the absence of surrounding topographical features makes reliable navigation systems crucial.

Currently, the global navigation satellite systems (GNSS) are the most widely used navigation systems [1]–[6], utilizing signals transmitted by satellites to provide PNT information. The U.S. Global Positioning System (GPS) is a well-known example of GNSS. However, GNSS has the disadvantage of being susceptible to radio frequency interference (RFI) [7]–[9] due to its weak signal reception strength. Additionally, GNSS is vulnerable to ionospheric anomalies [10]–[14]. Consequently, there is a growing interest in researching alternative

PNT (APNT) systems [15]–[29] that can be employed in situations where GNSS is unavailable.

Ranging Mode (R-Mode) [30]–[37] is an emerging alternative navigation technology in the marine field. It offers a terrestrial integrated navigation service that incorporates various components, including medium frequency (MF) R-Mode, very high frequency (VHF) data exchange system (VDES) R-Mode, and the existing terrestrial radio navigation system called enhanced long-range navigation (eLoran) [38]–[47].

Among these components, the positioning techniques of MF R-Mode and VDES R-Mode utilize the signals of opportunity (SOP) method [48]–[51]. This SOP method leverages the existing radio frequency (RF) signal infrastructure for positioning purposes. Specifically, MF R-Mode employs the differential GNSS (DGNSS) signals transmitted through MF bands, which provide GNSS correction information. On the other hand, VDES R-Mode utilizes VDES signals for digital communication within the VHF band.

The R-Mode study was initially launched in the EU's R-Mode Baltic project, and the performance of the initial study results was verified in the North Sea area [32]. The study revealed that MF R-Mode's pseudorange measurement performance was nearly 10 times worse at nighttime compared to daytime. The daytime period refers to the time from sunrise to sunset, while the nighttime period refers to the time from sunset to sunrise. The primary cause of this phenomenon is the skywave effect on the MF R-Mode signal, which occurs due to signal reflection in the ionosphere during propagation. Therefore, research on skywave detection and mitigation is essential to improve the performance of MF R-Mode and minimize its impact. However, determining the true occurrence of MF R-Mode skywave, which is crucial for conducting skywave studies, remains unaddressed. Consequently, there is a need to develop techniques and methodologies for generating the ground truth of skywave occurrence in the context of MF R-Mode.

In this study, we propose a skywave ground truth generation algorithm specifically designed for static scenarios, such as between a transmitter and a reference station, to investigate
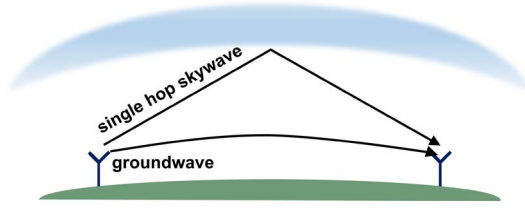
Fig. 1. Groundwave and skywave propagation path (modified from Fig. 1 of [37]).

MF R-Mode skywave detection techniques. Furthermore, we validate the feasibility of the proposed ground truth generation algorithm using experimental data transmitted from Chungju, South Korea, and received at the Daesan port, South Korea.

II. MF R-MODE SKYWAVE

The MF DGNSS signal employed in MF R-Mode is a signal transmitted from a DGNSS reference station. It contains GNSS correction information modulated using minimum shift keying (MSK) on a carrier within the 285–325 kHz frequency range. However, in MF R-Mode, the DGNSS signal is not used as is. Instead, two continuous wave (CW) signals are added to the null frequencies within the DGNSS MSK spectrum. In the case of the EU's R-Mode Baltic project [32], these frequencies were ± 250 Hz from the center frequency.

The generated MF R-Mode signal follows two primary propagation paths from a transmitter to a receiver. The first path is known as the groundwave, which is received when the transmitted signal propagates along the Earth's surface. The second path is called the skywave, received after reflection from the ionosphere, as shown in Fig. 1.

During the daytime, primarily the groundwave is received, while during nighttime, both the groundwave and skywave are received, resulting in a significant performance difference between day and night. This discrepancy can be attributed to the variations in the ionosphere between daytime and nighttime. In the MF frequency range, signals are mostly absorbed by the D layer of the ionosphere, which dissipates after sunset [52], [53]. Consequently, in the evening following sunset, the skywave is generated as signals are reflected by the E layer of the ionosphere. Due to the reflection in the ionosphere, the skywave follows a longer propagation path compared to the groundwave, resulting in increased propagation time and attenuation. The time delay of the skywave is represented in (1), where d is the distance between a transmitter and a receiver, h denotes the height of the ionosphere, and c represents the speed of light [37].

$$t_d = \frac{\sqrt{4h^2 + d^2} - d}{c}. \tag{1}$$

The received signal is represented in (2), which includes the groundwave along with the skywave reflected once in the ionosphere, known as the single-hop skywave [32].

$$
\begin{aligned}
r(t) &= s(t) + \alpha s(t - t_d) \\
&= B \sin(2\pi f t + \phi) + \alpha B \sin(2\pi f (t - t_d) + \phi) \quad (2) \\
&= \eta B \sin(2\pi f t + \phi + \beta).
\end{aligned}
$$

where $s(t)$ is the groundwave, $s(t - t_d)$ corresponds to the skywave, α denotes the attenuation factor, B denotes the amplitude of $s(t)$, f is the frequency, η is the amplitude scaling, and β is the phase shift. This equation demonstrates that when the skywave and groundwave are received together, the skywave introduces changes in both the amplitude and phase of the groundwave signal [32].

III. GROUND TRUTH GENERATION ALGORITHM

As mentioned in Section II, during daytime, the predominant signal received is the groundwave, while the skywave primarily occurs at nighttime, causing phase and amplitude variations. In this study, we propose a skywave ground truth generation algorithm specifically designed for static scenarios, such as between a transmitter and a reference station, with a particular focus on the rare occurrence of skywave during daytime. The algorithm is described in detail as Algorithm 1.

Algorithm 1: Skywave ground truth generation

Data: 1) phase data during daytime for three days, including the day before and after time t, Φ
      2) phase data at time t, ϕ_t

Result: existence of skywave at time t

$\mu_{day} \leftarrow \mathrm{avg}(\Phi)$
$\sigma_{day} \leftarrow \mathrm{std}(\Phi)$
$S \leftarrow |(\phi_t - \mu_{day})/\sigma_{day}|$
if $S \geq 4.5$ **then**
  | **return** true
end
return false

Since this is a ground truth generation algorithm, which identifies the actual occurrence of the skywave by post-processing, rather than a real-time skywave detection algorithm, both past and future data with respect to the time of interest can be used. To generate the skywave ground truth for the time of interest t, the phase data during the daytime is collected for a period of three consecutive days, including the day before and after time t. The daytime data is obtained from one hour after sunrise to one hour before sunset. The mean and standard deviation of the phase data during daytime for the three-day period are calculated. Subsequently, using these values, the Z-score of the phase measurement at time t is computed. Based on the calculated mean and standard deviation of the daytime data, if the absolute value of the Z-score exceeds 4.5, it indicates the presence of a skywave, representing an outlier in phase variation. Conversely, if the absolute value of the Z-score is below 4.5, it can be inferred that there is no skywave present.

Fig. 2. Receiver in the Daesan port.

IV. EXPERIMENT

A. Experimental Settings

The experimental verification of the algorithm was conducted by transmitting signals from Chungju, South Korea, and receiving them at the MF R-Mode continuously operating reference station (CORS) located near the Daesan port. Fig. 2 illustrates the experimental setup at the CORS in the Daesan port. The MSK signal transmitted from the Chungju station has a frequency of 318 kHz, while the CW signals have frequencies centered at 318 kHz ± 450 Hz. In contrast to the EU's R-Mode Baltic project, CW signals were added at ±450 Hz from the center frequency to achieve a wider separation between the CW signals.

The receiver used in the experiment is the "MFR-1a Medium Frequency R-Mode Receiver" by Serco, which was also used in [34]. The experiment was performed from February 11th to 13th, 2023. Using the proposed Algorithm 1, the ground truth of skywave occurrence in the data on the 12th was computed. On February 11th, the sunrise time at the Daesan port was approximately 7:30 AM, and the sunset time was around 6:10 PM. For the period from February 11th to 13th, the daytime data used in the experiment spanned from 8:30 AM to 8:00 PM.

B. Experimental Result

Fig. 3 shows the results of determining skywave ground truth using the measured phase of the CW1 signal at 317.55 kHz and the CW2 signal at 318.45 kHz at the Daesan port. The blue dots represent the measured phase data, while the orange dots indicate the presence of skywave obtained by the ground truth generation algorithm.
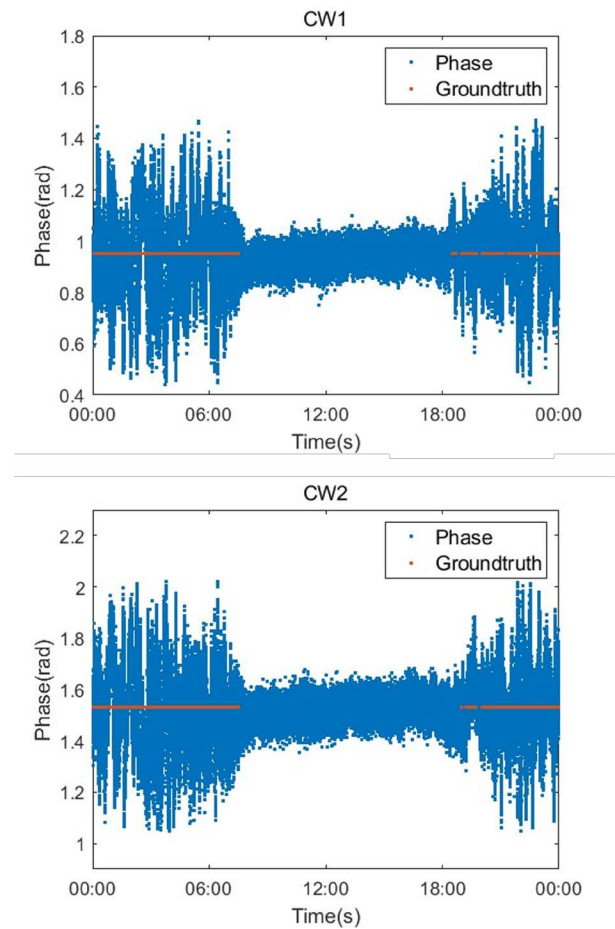

Fig. 3. Experimental result.

V. CONCLUSION

In this paper, we proposed a skywave ground truth generation algorithm that is essential for studying the mitigation of the significant error factor caused by skywave interference in the MF R-Mode system. The algorithm was developed based on the observation that skywave phenomena are mainly present during nighttime, accompanied by phase variations, while being largely absent during daytime. The validation of the proposed algorithm was performed using MF R-Mode CW1 and CW2 signals transmitted from Chungju, South Korea, and received at the Daesan port.

REFERENCES

[1] P. Misra and P. Enge, *Global Positioning System: Signals, Measurements, and Performance*. Ganga-Jamuna Press, 2011.

[2] D. De Lorenzo, S. Lo, J. Seo, Y.-H. Chen, and P. Enge, "The WAAS/L5 signal for robust time transfer: Adaptive beamsteering antennas for satellite time synchronization," in *Proc. ION GNSS*, 2010, pp. 2106–2116.

[3] Y.-H. Chen, J.-C. Juang, D. De Lorenzo, J. Seo, S. Lo, P. Enge, and D. Akos, "Real-time dual-frequency (L1/L5) GPS/WAAS software receiver," in *Proc. ION GNSS*, 2011, pp. 767–774.

[4] K. Park, W. Kim, and J. Seo, "Effects of initial attitude estimation errors on loosely coupled smartphone GPS/IMU integration system," in *Proc. ICCAS*, 2020, pp. 800–803.

[5] W. Kim and J. Seo, "Low-cost software-defined GPS simulator with the capability of time synchronization," in *Proc. ICCAS*, 2018, pp. 1087–1090.

[6] H. Lee, J. Seo, and Z. Kassas, "Urban road safety prediction: A satellite navigation perspective," *IEEE Intell. Transp. Syst. Mag.*, vol. 14, no. 6, pp. 94–106, Nov.-Dec. 2022.

[7] K. Park and J. Seo, "Single-antenna-based GPS antijamming method exploiting polarization diversity," *IEEE Trans. Aerosp. Electron. Syst.*, vol. 57, no. 2, pp. 919–934, Apr. 2021.

[8] K. Park, D. Lee, and J. Seo, "Dual-polarized GPS antenna array algorithm to adaptively mitigate a large number of interference signals," *Aerosp. Sci. Technol.*, vol. 78, pp. 387–396, Jul. 2018.

[9] S. Kim, K. Park, and J. Seo, "Mitigation of GPS chirp jammer using a transversal FIR filter and LMS algorithm," in *Proc. ITC-CSCC*, 2019.

[10] J. Lee, Y. Morton, J. Lee, H.-S. Moon, and J. Seo, "Monitoring and mitigation of ionospheric anomalies for GNSS-based safety critical systems," *IEEE Signal Process Mag.*, vol. 34, no. 5, pp. 96–110, Sep. 2017.

[11] M. Kim, J. Seo, and J. Lee, "A comprehensive method for GNSS data quality determination to improve ionospheric data analysis," *Sensors*, vol. 14, no. 8, pp. 14 971–14 993, Aug. 2014.

[12] H. Lee, S. Pullen, J. Lee, B. Park, M. Yoon, and J. Seo, "Optimal parameter inflation to enhance the availability of single-frequency GBAS for intelligent air transportation," *IEEE Trans. Intell. Transp. Syst.*, vol. 23, no. 10, pp. 17 801–17 808, Oct. 2022.

[13] A. K. Sun, H. Chang, S. Pullen, H. Kil, J. Seo, Y. J. Morton, and J. Lee, "Markov chain-based stochastic modeling of deep signal fading: Availability assessment of dual-frequency GNSS-based aviation under ionospheric scintillation," *Space Weather*, vol. 19, no. 9, pp. 1–19, Sep. 2021.

[14] N. Ahmed and J. Seo, "Statistical evaluation of the multi-frequency GPS ionospheric scintillation observation data," in *Proc. ICCAS*, 2017, pp. 1792–1797.

[15] Y. Li, Y. Hua, B. Yan, and W. Guo, "Research on the eLoran differential timing method," *Sensors*, vol. 20, p. 6518, 2020.

[16] M. Jia, H. Lee, J. Khalife, Z. M. Kassas, and J. Seo, "Ground vehicle navigation integrity monitoring for multi-constellation GNSS fused with cellular signals of opportunity," in *Proc. IEEE ITSC*, 2021, pp. 3978–3983.

[17] S. Jeong, H. Lee, T. Kang, and J. Seo, "RSS-based LTE base station localization using single receiver in environment with unknown path-loss exponent," in *Proc. ICTC*, 2020, pp. 958–961.

[18] S. Han, T. Kang, and J. Seo, "Smartphone application to estimate distances from LTE base stations based on received signal strength measurements," in *Proc. ITC-CSCC*, 2019.

[19] H. Lee, J. Seo, and Z. Kassas, "Integrity-based path planning strategy for urban autonomous vehicular navigation using GPS and cellular signals," in *Proc. ION GNSS+*, 2020, pp. 2347–2357.

[20] J. Rhee and J. Seo, "Low-cost curb detection and localization system using multiple ultrasonic sensors," *Sensors*, vol. 19, no. 6, Mar. 2019.

[21] ——, "Ground reflection elimination algorithms for enhanced distance measurement to the curbs using ultrasonic sensors," in *Proc. ION ITM*, 2018, pp. 224–231.

[22] E. Kim and J. Seo, "SFOL pulse: A high accuracy DME pulse for alternative aircraft position and navigation," *Sensors*, vol. 17, no. 10, Sep. 2017.

[23] S. Lee, E. Kim, and J. Seo, "SFOL DME pulse shaping through digital predistortion for high-accuracy DME," *IEEE Trans. Aerosp. Electron. Syst.*, vol. 58, no. 3, pp. 2616–2620, Jun. 2022.

[24] Y. Shin, S. Lee, and J. Seo, "Autonomous safe landing-area determination for rotorcraft UAVs using multiple IR-UWB radars," *Aerosp. Sci. Technol.*, vol. 69, pp. 617–624, Oct. 2017.

[25] J. Kim, J.-W. Kwon, and J. Seo, "Simulation study on a method to localize four mobile robots based on triangular formation," in *Proc. ION Pacific PNT*, 2017, pp. 348–361.

[26] H. Lee, T. Kang, S. Jeong, and J. Seo, "Evaluation of RF fingerprinting-aided RSS-based target localization for emergency response," in *Proc. IEEE VTC*, Jun. 2022, pp. 1–7.

[27] T. Kang and Y. Shin, "Indoor navigation algorithm based on a smartphone inertial measurement unit and map matching," in *Proc. ICTC*, 2021, pp. 1421–1424.

[28] W. Kim and J. Seo, "Low-cost GNSS simulators with wireless clock synchronization for indoor positioning," *IEEE Access*, vol. 11, pp. 55 861–55 874, 2023.

[29] H. Lee and J. Seo, "Performance comparison of numerical optimization algorithms for RSS-TOA-based target localization," in *Proc. IEEE VTC*, Jun. 2023, pp. 1–6.

[30] G. Johnson, P. Swaszek, J. Alberding, M. Hoppe, and J.-H. Oltmann, "The feasibility of R-Mode to meet resilient PNT requirements for e-Navigation," in *Proc. ION GNSS*, 2014, pp. 3076–3100.

[31] G. Johnson and P. Swaszek, "Feasibility study of R-Mode combining MF DGNSS, AIS, and eLoran transmissions," German Federal Waterways and Shipping Administration, Tech. Rep., 2014.

[32] ——, "Feasibility study of R-Mode using MF DGPS transmissions," German Federal Waterways and Shipping Administration, Final Report, Tech. Rep., 2014.

[33] G. W. Johnson, P. F. Swaszek, M. Hoppe, A. Grant, and Šafář, "Initial results of MF-DGNSS R-Mode as an alternative position navigation and timing service," in *Proc. ION ITM*, 2017, pp. 1206–1226.

[34] G. Johnson, K. Dykstra, S. Ordell, and P. Swaszek, "R-Mode positioning system demonstration," in *Proc. ION GNSS*, 2020, pp. 839–855.

[35] P.-W. Son, J. Park, J. Yu, S. Jeong, Y. Han, and T. H. Fang, "Skywave detection and mitigation for the MF R-Mode continuously operating reference station," *Sensors*, vol. 23, no. 11, pp. 1–14, 2023.

[36] P. F. Swaszek, R. J. Hartnett, and G. W. Johnson, "Ranging/timing off of the NDGPS signal: Potential performance," in *Proc. ION ITM*, 2012, pp. 452–461.

[37] S. Jeong and P.-W. Son, "Development of an R-Mode simulator using MF DGNSS signals," in *Proc. ICCAS*, 2021, pp. 1104–1108.

[38] P.-W. Son, J. Rhee, J. Hwang, and J. Seo, "Universal kriging for Loran ASF map generation," *IEEE Trans. Aerosp. Electron. Syst.*, vol. 55, no. 4, pp. 1828–1842, Oct. 2019.

[39] P.-W. Son, J. Rhee, and J. Seo, "Novel multichain-based Loran positioning algorithm for resilient navigation," *IEEE Trans. Aerosp. Electron. Syst.*, vol. 54, no. 2, pp. 666–679, Oct. 2018.

[40] W. Kim, P.-W. Son, S. G. Park, S. H. Park, and J. Seo, "First demonstration of the Korean eLoran accuracy in a narrow waterway using improved ASF maps," *IEEE Trans. Aerosp. Electron. Syst.*, vol. 58, no. 2, pp. 1492–1496, Apr. 2022.

[41] J. H. Rhee, S. Kim, P.-W. Son, and J. Seo, "Enhanced accuracy simulator for a future Korean nationwide eLoran system," *IEEE Access*, vol. 9, pp. 115 042–115 052, Aug. 2021.

[42] P. Williams and C. Hargreaves, "UK eLoran–Initial operational capability at the Port of Dover," in *Proc. ION ITM*, 2013, p. 392–402.

[43] P.-W. Son, S. G. Park, Y. Han, K. Seo, and T. H. Fang, "Demonstration of the feasibility of the Korean eLoran system as a resilient PNT in a testbed," *Remote Sens.*, vol. 15, no. 14, pp. 1–12, 2023.

[44] J. Hwang, P.-W. Son, and J. Seo, "TDOA-based ASF map generation to increase Loran positioning accuracy in Korea," in *Proc. IEEE ICCE-Asia*, 2018.

[45] P.-W. Son, J. Rhee, Y. Han, K. Seo, and J. Seo, "Preliminary study of multichain-based Loran positioning accuracy for a dynamic user in South Korea," in *Proc. IEEE/ION PLANS*, 2018, pp. 1034–1038.

[46] P.-W. Son, S. G. Park, K. Seo, S. Park, and T. H. Fang, "Preliminary study of the re-radiation effect of loran signal to improve the positioning accuracy," in *Proc. ENC*, 2019, pp. 1–4.

[47] P.-W. Son, S. G. Park, Y. Han, and K. Seo, "eLoran: Resilient positioning, navigation, and timing infrastructure in maritime areas," *IEEE Access*, vol. 8, pp. 193 708–193 716, 2020.

[48] J. A. McEllroy, "Navigation using signals of opportunity in the AM transmission band," Master's thesis, Air Force Institute of Technology, 2006.

[49] P. Wang, Y. Wang, and Y. J. Morton, "Signal tracking algorithm with adaptive multipath mitigation and experimental results for LTE positioning receivers in urban environments," *IEEE Trans. Aerosp. Electron. Syst.*, vol. 58, no. 4, pp. 2779–2795, 2022.

[50] C. Huang, H. Qin, C. Zhao, and H. Liang, "Phase-time method: Accurate doppler measurement for iridium NEXT signals," *IEEE Trans. Aerosp. Electron. Syst.*, vol. 58, no. 6, pp. 5954–5962, 2022.

[51] Y. Yang, J. Khalife, J. J. Morales, and Z. M. Kassas, "UAV waypoint opportunistic navigation in GNSS-denied environments," *IEEE Trans. Aerosp. Electron. Syst.*, vol. 58, no. 1, pp. 663–678, Feb. 2022.

[52] R. Bureau, "The ionosphere and its effects on radiowave propagation," International Telecommunication Union, Tech. Rep., 1998.

[53] D. C. Poppe, *Coverage and performance prediction of DGPS systems employing radiobeacon transmissions*. Bangor University (United Kingdom), 1995.